Soil Dynamics and Earthquake Engineering 166 (2023) 107743

Contents lists available at ScienceDirect

Soil Dynamics and Earthquake Engineering

journal homepage: www.elsevier.com/locate/soildyn

A signal-processing approach to assess viscous-damper absorbing boundary conditions for dry and saturated soils in time domain dynamic problems

Juana Arias-Trujillo [a,*], Susana López-Querol [b]

[a] Universidad de Extremadura, School of Engineering Department of Construction, Avda. de la Universidad, s/n, 10003 Caceres, Spain
[b] University College London, Department of Civil, Environmental and Geomatic Engineering, London WC1E 6BT, United Kingdom

ARTICLE INFO

Keywords:
Viscous dampers
Digital signal schemes
Directional spectrum
Paserval's relation
Spectral coherence
Time-domain finite element models

ABSTRACT

For numerical modelling of dynamic problems, absorbing boundary conditions (ABC) are necessary to attenuate reflected waves ('box effect'). Different approaches have been developed for this numerical issue, being the viscous damper (VD-ABC) widely employed. The VD-ABC is not frequency dependent but a total attenuation is never achieved, and hence a tentative enlargement of the computational domain is adopted. Relevant issues on VD-ABC are integrative assessment by a signal processing approach. One and two-phases (dry and saturated soil, respectively) time-domain responses have been considered besides spectral properties and energy content. P-wave velocity has been modified to consider the fluid bulk modulus. ABC affect differently to each variable, being the vertical displacement the less sensible. Higher frequencies present great discrepancies although their energy contribution to the overall signal is not relevant. The results with VD-ABC yield to a feasible reduction of the size of the computational domain, maintaining the required accuracy.

1. Introduction

In dynamic finite element models (FEM), artificial boundary schemes are necessary to simulate the continuity of the media and modelling the radiation of energy outwards of the truncated and finite computational domain. The use of fixed conditions (displacements restricted) is inappropriate because of the spurious oscillations that are reintroduced into the computational domain, when the no-damped waves in the media reach the boundaries, generating reflected waves ('box effect'). This effect can seriously alter the computed solution in the area of interest. Nowadays, this numerical drawback has not been completely solved, and different numerical approaches are continuously being developed for addressing this issue from different frameworks and scopes [1–7].

Focusing on time-domain FEM, they are mainly called as 'absorbing boundary' (ABC), but other denominations can be found in the literature ('Transmitting Boundary', 'Silent Boundary', 'Radiating Boundary', 'Transparent Boundary', 'Quiet Boundary', 'Non-reflecting Boundary' among others). Despite the published approaches, a predominant methodology for ABC is not established yet, and the pioneer viscous-damper ABC proposed by Lysmer and Kuhlemeyer [8] is the most widely employed nowadays. Moreover, several approaches formulated by other researchers derive into the viscous-damper formulation in some cases. On the other hand, the researches developed for two-phases media, such as saturated soils, are very limited.

Artificial boundaries can be placed far enough from the area of interest of the model ('Extended boundary'), in order to attenuate the waves by means of the material damping, before they reach the boundaries. However, this usually implies a significant increment of the computational effort. Usually, an suitable ABC scheme and a moderate extension of the domain are employed together for assuring the accuracy and computational efficiency of the model. The selection of the proper computational domain size is also a relevant task in this topic. In common practice, a few random time-histories are usually compared to fit the domain. For fixed boundary conditions, it is expected that the computed solution improves with the increment of the computational domain. However, when ABC are applied, it is not easy to verify whether an enlargement of the domain implies a relevant improvement on the result or not, despite the increment in the computational cost. In both cases, the comparison of time-history responses can be tedious and not enlightened because multiple waves can be superposed, especially in problems with complex loads.

In this research, a signal processing approach has been applied to analyse the influence of the viscous-damper ABC in dry and saturated problems ($u - p_w$ Biot's formulation). For saturated problem, the p-wave velocity has been modified by means of the bulk modulus of the fluid according to the expression developed by Yang [9], which can be implemented in any standard FEM code. According to the

* Corresponding author.
E-mail addresses: jariastr@unex.es (J. Arias-Trujillo), s.lopez-querol@ucl.ac.uk (S. López-Querol).

https://doi.org/10.1016/j.soildyn.2022.107743
Received 9 October 2022; Received in revised form 27 December 2022; Accepted 27 December 2022
Available online 6 January 2023

literature, the efficiency of this viscous-damper ABC is affected by the angle of incidence of the waves in the boundary. However, complex phenomena of interaction between the waves in the medium and with the boundaries progressively transform the resulting signal when it arrives to the area of engineering interest, which is normally far enough from the boundaries. To analyse these complex wave transformation processes, almost 9000 time-history responses have been monitored in a spatial grid for different types of variables (displacement, stress and pore pressure). Each time-history has been treated like a signal using the following signal processing schemes: amplitude and phase response spectra, directional spectra, energy content by the Parseval's relation, bandwidth and spectral coherence. A suitable numerical model has been developed, preventing the attenuation of the waves by other damping sources, and considering four computational domain sizes (small, intermediate, large and huge) for comparison purposes. In summary, three relevant novelties can be highlighted in this research: 1. the generalization of viscous dampers for two-phase media (saturated soil), supported on a modification of the p-wave velocity by considering the fluid bulk modulus in a u-pw Biot's formulation; 2. the influence of the viscous dampers on each response variables (stress, displacement or pore pressure), which has not been systematically analysed before in the literature; and finally, 3. the influence of each variable on this numerical issue in the time-histories of each variable, such as the enlargement of the computational domain, distance and orientation of the boundaries (rather than the angle of incidence only), which represent an integrative assessment attending the spectral properties and energy content of each response by means of a signal-processing approach, in both dry and saturated problems.

This paper is organized as follows: first, a literature review is presented, where the general techniques to approach ABC for one and two-phase media are presented. After that, the generalization of viscous dampers ABC in saturated media for coupled $u-p_w$ formulation adopted in this research is described, describing its numerical implementation in a FEM code and the corresponding validation examples. Then, the responses of viscous dampers ABC are analysed by a specific numerical model. The corresponding time-history responses are jointly analysed from a signal processing approach. Finally, the most relevant conclusions derived from this research are highlighted.

2. Literature review

In a semi-infinite elastic media subject to dynamic loading, two types of waves, body (longitudinal or P-waves and transverse or S-waves) and surface, can be propagated [10]. For the numerical treatment of the artificial boundaries, aiming to reduce the spurious reflected waves on the boundaries, mainly P-waves and S-waves are considered. A brief review of the main reported procedures to avoid these reflections is presented next, including those specific for saturated porous media.

2.1. General techniques to approach ABC for one-phase media

In the literature, different numerical techniques can be found to implement absorbing boundary conditions (ABC) both for frequency-domain problems and for time-domain problems, which is the framework considered in the present research.

The pioneer work developed by Lysmer and Kuhlemeyer [8] is the most successful and widely employed methodology nowadays [11,12]. They used viscous damping forces by means of viscous dampers located on the boundaries to try to absorb those longitudinal and transverse waves that reach the boundary, avoiding (or reducing) the reflection of energy into the computational domain. The efficiency of this technique does not depend on the frequency content of the waves, but on the angle of incidence of the body waves on the boundaries. When waves incise normally to the boundary, the ABC proposed by Lysmer and Kuhlemeyer presents a perfect absorption, and almost perfect when the angle is higher than 30°. Slight reflections occur for lower angles of incidence, although they have been scarcely quantified in the literature for 2D problems [8,11].

Later, Smith [13] proposed an alternative technique regardless of frequency-content or angle of incidence of the waves, based on the superposition of the solution obtained from two opposite 2D-problems with different boundary conditions, so the reflected waves are cancelled. This procedure requires an enormous computational cost and implies linear responses.

Clayton and Engquist [14] extrapolated the 'Paraxial Boundary' to a two-dimensional scalar and elastic wave equation, Eq. (1):

$$\left(\frac{\partial^2}{\partial x^2}+\frac{\partial^2}{\partial z^2}-\frac{1}{v^2}\frac{\partial^2}{\partial t^2}\right)u=0 \tag{1}$$

where v is the velocity of the wave, u is the displacement, x and z are the spacial coordinates, and t is the time. After solving this equation, two waves with equal amplitude and opposite direction of propagation are obtained: one wave goes out of the domain whereas the other one goes in. The target of a paraxial approximation is to find a differential equation to allow the development of the out-waves only, neglecting the in-waves.

After the solution of Eq. (1), the wave number k_x (Eq. (2)) is obtained, where ω is the angular frequency of the wave, k_x and k_z are the wave numbers in x and z, respectively, and the sign $\pm$ corresponds to the in-wave and out-wave. The sign associated to the in-wave must be chosen to cancel it ($k_x=0$). The term $\left(\frac{vk_z}{\omega}\right)$ can be approximated with different orders, resulting in the paraxial boundary condition. It must be highlighted that for a first-order approximation, this approach coincides with the viscous-dampers conditions proposed by Lysmer and Kuhlemeyer [8]. For higher-order of approximations, numerical instabilities can appear though. This technique is convenient for finite difference models.

$$k_x=\pm\frac{\omega}{v}\sqrt{1-\left(\frac{vk_z}{\omega}\right)^2} \tag{2}$$

For finite element models, Liao and Wong [15] proposed the methodology known as 'Extrapolation Boundary' which is based on a prediction of the boundary displacement computed from an extrapolation of the displacements of the surrounding points. This method is also related with the concept of paraxial approximation but avoiding its numerical instabilities, although a large amount of data must be stored and it could fail when several waves arrive to the boundary at the same time.

Higdon [16] proposed the 'Multi-directional Boundary' which is based on a collection of first-order differential operators. This type of boundary allows a total absorption of the waves for some particular angles of incidence. By means of the multiplication of several differential operators this formulation can be generalized to waves with other angles of incidence. For some particular case, this method coincides to the paraxial approximation. In practice, only the product of two or three operators is possible, since the reiterative use of higher-order difference operators is complex to define in an FEM, and moreover, it could trigger in instability issues. Therefore, 'Multi-directional Boundary' does not result in a practical relevant advance, in terms of its accuracy respect to others techniques, despite of its complex implementation.

Other researchers like Givoli and Hagstrom [17–20] have proposed different approaches to achieve a non-reflecting boundary conditions of any order ('High-order ABC') avoiding the issues pointed out by the Higdon's formulation. A review of this high-order methods can be found in [21].

'Perfectly Matched Layers' (PML) [22] is another relevant and alternative technique, developed originally for electromagnetic waves. In this approach, an extra additional layer surrounding the computational domain is added, with the aim of causing an exponential decay of the out-waves when they come in this layer, avoiding reflected-waves. Any frequency or angle of incidence can be absorbed. This method has

mainly been used in frequency-domain problems, although researchers like Basu and Chopra [23] tried to expand it to the time-domain. The accuracy of 'PML' is higher than the conventional viscous boundary although its computational cost increases from 1.5 to 1.75 times and can be inaccurate for some particular types of waves [11,23].

Researchers like Rabinovich et al. [20,24] or Lancioni [22] compared the 'PML' with the 'High-order ABC' for a 1D-problem both in the frequency-domain and time-domain, concluding that, in general, 'High-order ABC' are more accurate than 'PML', and its computational cost is lower. However, the numerical implementation of 'PML' in a finite element code is easier, whereas the implementation of the 'High-order ABC' is not trivial, since some modifications of a standard code are necessary and an especial treatment of the corners of the domain are necessary.

2.2. Approaches for ABC in saturated porous media

ABC in saturated porous media have been scarcely investigated in comparison with solid media or dry soils. A wide review was published by Zerfa and Loret [25]. Several approaches are reported in the literature but none of them clearly predominates yet.

In a two phases medium (solid and fluid), three types of waves can appear, two longitudinal and one transverse [26]. The velocity of the first longitudinal wave (the highest velocity) depends on the elastic modulus (E) and Poisson's coefficient (ν), whereas the velocity of the second longitudinal wave depends on loading frequency and permeability. This second wave is usually neglected because it is quickly attenuated with depth and dissipates energy by diffusion [25–27].

Degrande and Roeck [28,29] developed an ABC for dynamic problems in saturated media supported on the Biot's formulation, trying to cancel the amplitude of the reflected waves and establish a relationship between effective stress and pore pressure with the displacement of the boundary. These ABC are frequency-dependent so they are suitable for frequency domain problems. For the first longitudinal wave, they verified that the solid phase and pore pressure displacements are in-phase, whereas they are out of phase for the second longitudinal wave which is attenuated. For low-frequency input loads, there is an important viscous coupling between the solid and fluid phases, and therefore, the two-phase medium behaves similarly to a one-phase medium, neglecting the relative displacement of the fluid phase respect to the solid, and therefore the resulting ABC are equivalent to the viscous-dampers proposed by Lysmer and Kuhlemeyer [8]. On the other hand, for a loading with high-frequency content, the viscous coupling between phases disappears and the saturated porous medium behaves like a non-dissipative porous medium.

Modaressi and Benzenati [27] applied the previously discussed paraxial approximation to saturated porous media through the Biot's theory, with the $u-p_w$ formulation in a frequency-domain framework. They assumed a linear elastic response and that the permeability is constant and non-frequency dependent obtaining three waves, two longitudinal (v_{p_1}, v_{p_2}) and one transverse (v_s), Eq. (3).

$$\begin{aligned} v_{p_1}^2 &= C_p^2\left[1+\frac{Q^*}{\lambda+2\mu}\right] \\ v_{p_2}^2 &= i\omega k' Q^*\left[\frac{\lambda+2\mu}{\lambda+2\mu+Q^*}\right] \\ v_s^2 &= C_s^2 \end{aligned} \tag{3}$$

where $C_p^2=(\lambda+2\mu)/\rho$, $C_s^2=\mu/\rho$ and $\rho=(1-n)\rho_s+n\rho_f$; λ and μ are the elastic Lame constants; Q^* is the coupled soil–fluid compressibility; k' is the permeability; n is the porosity; ρ_s and ρ_f are the solid particle and fluid density, respectively; ω is the angular frequency and i denotes the imaginary number.

When the quotient is $Q^*/(\lambda+2\mu)\gg 1$, two longitudinal waves propagate in the medium. The first P-wave (v_{p_1}) does not depend on the frequency and can be defined similar to C_p plus a complementary term which depends on soil–fluid compressibility. The second P-wave (v_{p_2}) is attenuated and its velocity is proportional to the square of the angular frequency of the solicitation and the permeability. When the quotient is $Q^*/(\lambda+2\mu)\ll 1$, the first P-wave travels with a velocity equivalent to the longitudinal wave in a one-phase medium, while the second P-wave is attenuated too, and the velocity is proportional to the permeability, the frequency and the fluid compressibility.

According to the Modaressi and Benzenati's proposal, Akiyoshi et al. [30] extrapolated the paraxial approximation to other formulations ($u-p_w$, u-w, u-U), and to a non-linear 2D problem obtaining satisfactory results even in problems with high non-linearities. In both researches, despite the followed approach, the ABC obtained keep some similarities to the viscous-dampers.

Gajo et al. [31] developed a 'Multidirectional absorbing boundary' for a two-phase elastic saturated porous medium, with an u-U formulation based on the Biot's theory. They analysed two extreme cases, with high and low permeabilities. In the case of high-permeability, where the high-frequency content is relevant and the viscous coupling between solid and fluid phases is low, two longitudinal and one transverse waves develop. In the case of low-permeability, where the high-frequency content is less relevant, the solid–fluid viscous coupling is high and the medium behaves like a one-phase, and only one longitudinal and one transverse waves appear. Similar behaviour were outlined by other researchers [26,28,29]. The transition between high and low coupling states occurs for a short range of permeabilities and frequency-contents, hence the modifications in the wave velocities are very limited, and the possible spurious reflections are low for intermediate cases. For high permeability, the velocity of the wave does not depend on the frequency. For low permeability, where the porous medium behaves like one-phase, the results coincide with the approaches proposed by Lysmer and Kuhlemeyer [8], and also with Akiyoshi [30] and Modaressi and Benzenati [27].

Zerfa and Loret [25] proposed to apply viscous stresses on the absorbing boundaries, assuming an elastic linear isotropic behaviour for the boundaries, in saturated porous media in the time-domain and u-w formulation with non-frequency dependent velocity of the waves. The contribution of the second longitudinal wave is not neglected and the general case for a high-permeability medium is developed. Dry soil or low-permeability (undrained) cases are obtained as particular solutions. The definition of the velocity of the waves for the undrained case is equivalent to the expression proposed by Gajo et al. [31].

3. Generalization of viscous dampers-ABC in saturated media for coupled $u-p_w$ formulation

A $u-p_w$ formulation supported on Biot's theory is presented to outline the generalization of the ABC for saturated porous media proposed in this research. The numerical scheme has been implemented in the academic FEM-code GeHoMadrid (GHM) [32]. The $u-p_w$ formulation proposed by Zienkiewicz et al. [33–35] for solving the Biot's equations by means of the finite element method is adopted herein. The fluid acceleration relative to the solid skeleton is neglected, thus the absolute displacement of the solid phase (u) and pore water pressure (p_w) are the governing variables in this formulation, which is neither acceptable for very high-frequencies content or impact loading problems, nor nearly incompressible material. After the corresponding spacial discretization, a Newmark time-step integration algorithm is employed, using a second-order differential scheme for displacement and a first-order for pore pressure [36,37]. The resulting system is shown in Eqs. (4) to (7), which are coupled by the matrix $[Q]$ and where $\Delta\ddot{\vec{u}}$ and $\Delta\dot{\vec{p}}$ are the unknowns that can be iteratively solved after each time-step according to Eqs. (8) to (12). In the case of dry soil, Eq. (5) and the term $[Q]$ are omitted.

$$\left([M]+\gamma\Delta t\,[C]+\beta\Delta t^2\,[K]\right)\Delta\ddot{\vec{u}}_n-(\theta\Delta t\,[Q])\,\Delta\dot{\vec{p}}_n=\left\{-G^u_{n+1}\right\} \tag{4}$$

$$\left(\theta\Delta t\,[Q]^T\right)\Delta\ddot{\vec{u}}_n+\left(\frac{\theta}{\gamma}\,[S]+\frac{\theta^2\Delta t\,[H]}{\gamma}\right)\Delta\dot{\vec{p}}_n=\left\{-\frac{\theta}{\gamma}G^p_{n+1}\right\} \tag{5}$$

where:

$$\{G^{u}_{n+1}\} = [M]\,\ddot{\bar{u}}_{n+1} + [C]\,\dot{\bar{u}}_{n+1} - [Q]\,\bar{p}_{n+1} + \int_{\Omega} [B]^{T}\,\sigma'_{n+1}\,d\Omega - \{f^{u}_{n+1}\} \quad (6)$$

$$\left\{G^{p}_{n+1}\right\} = [Q]^{T}\,\dot{\bar{u}}_{n+1} + [H]\,\bar{p}_{n+1} + [S]\,\dot{\bar{p}}_{n+1} - \left\{f^{p}_{n+1}\right\} \quad (7)$$

$$\ddot{\bar{u}}_{n+1} = \ddot{\bar{u}}_{n} + \Delta\ddot{\bar{u}}_{n} \quad (8)$$

$$\dot{\bar{u}}_{n+1} = \dot{\bar{u}}_{n} + \ddot{\bar{u}}_{n}\Delta t + \gamma\Delta\ddot{\bar{u}}_{n}\Delta t \quad (9)$$

$$\bar{u}_{n+1} = \bar{u}_{n} + \dot{\bar{u}}_{n}\Delta t + \frac{1}{2}\ddot{\bar{u}}_{n}\Delta t^{2} + \beta\Delta\ddot{\bar{u}}_{n}\Delta t^{2} \quad (10)$$

$$\dot{\bar{p}}_{n+1} = \dot{\bar{p}}_{n} + \Delta\dot{\bar{p}}_{n} \quad (11)$$

$$\bar{p}_{n+1} = \bar{p}_{n} + \dot{\bar{p}}_{n}\Delta t + \theta\Delta\dot{\bar{p}}_{n}\Delta t \quad (12)$$

$[M]$, $[C]$, $[K]$, $[Q]$, $[H]$ and $[S]$ are the mass, the viscous damping, the stiffness, the coupling, the permeability and the compressibility matrices, respectively. $\{f^{u}\}$ and $\{f^{p}\}$ are the force vectors for the solid phase and the fluid phase, whereas $\bar{u}$ and $\bar{p}$ are the global displacement and pore pressure vectors, respectively. The integral term corresponds to the effective stress and the matrix with the derive of the shape functions. The dots over each variable refer to the order of derivative and the subindices n and $n+1$ refer to the previous and current time-steps, where the time (t) is defined as $t_{n+1} = t_n + \Delta t$, with Δt the time-step. The superindices u and p refers to soil displacement or pore pressure, respectively. The variables γ, β and θ are the Newmark's time-integration coefficients.

3.1. Velocity of waves in saturated media

The ABC considered in this research are based on the viscous damper approach originally proposed by Lysmer and Kuhlemeyer [8], generalized to saturated porous media by means of a modification of the velocity of the first longitudinal wave according to the expressions developed by Yang [9], where the compressional wave velocity is linked with the Skempton's pore pressure coefficient. The proposed formulation for time-domain problems is equivalent to the paraxial approximation employed by Modaressi and Benzenati [27] in the frequency-domain. For a dry soil, this ABC coincides with the original Lysmer and Kuhlemeyer's proposal.

Lysmer and Kuhlemeyer [8] proposed a viscous-dampers located in all the degrees of freedom of the boundary elements, trying to simulate the wave radiations out of the domain. In FEM, they are modelled by means of normal and shear stresses, Eqs. (13) and (14), applied along the boundary of the computation domain [38], which depend on the velocities of the waves. As exposed, in soil dynamics problems, the second longitudinal wave can be neglected since it tends to be attenuated for low-frequency problems [9,26], which is also consistent with the $u-p_w$ formulation considered herein. Therefore, a compressive wave which propagates in both solid and fluid phases, and a transverse wave, which propagates only in the solid phase, must be absorbed by the artificial boundaries numerical schemes.

$$\sigma = \rho v_p \dot{u}_n \quad (13)$$

$$\tau = \rho v_s \dot{u}_t \quad (14)$$

where σ and τ are the normal and the shear stress on the boundaries of the model, respectively; $\dot{u}_n$ and $\dot{u}_t$ are the normal and the tangential velocity of the medium, respectively; v_p is the compressive wave velocity; v_s is the shear wave velocity and ρ is the density of the medium.

For a solid medium or dry soil, the velocities of the waves are computed as Eqs. (15) and (16), where E is the modulus of elasticity, G is the shear modulus, ν is the Poisson's ratio and K_b is the bulk modulus defined as $K_b = \frac{E}{3(1-2\nu)}$.

$$v_p = \sqrt{\frac{E(1-\nu)}{(1-2\nu)(1+\nu)\rho}} = \sqrt{\frac{K_b + \frac{4}{3}G}{\rho}} \quad (15)$$

$$v_s = \sqrt{\frac{G}{\rho}} = \sqrt{\frac{E}{2(1+\nu)\rho}} \quad (16)$$

For a saturated medium, the expression for the compressive wave velocity obtained by Yang [9], from Skempton's pore pressure parameter (B), has been adopted according to Eq. (17). Comparing Eqs. (17) to (15), the coupled soil–fluid compressibility is considered respect to the dry case, which is simplified as K_f/n for fully saturated porous medium with incompressible particles [9], where K_f is the bulk modulus of the pore water, n is the porosity, and ρ_{sat} is the density of the medium given by Eq. (18), where ρ_s and ρ_f denote the density of the soil particles and fluid, respectively. Since the S-waves do not propagate by a fluid phase, the velocity of the transverse wave is computed by Eq. (16) regardless the type problem.

$$v_p = \sqrt{\frac{K_b + \frac{4}{3}G + \frac{K_f}{n}}{\rho_{sat}}} \quad (17)$$

$$\rho_{sat} = (1-n)\rho_s + n\rho_f \quad (18)$$

3.2. Numerical implementation

The numerical implementation of the ABC described in a standard finite element code is outlined. The corresponding coefficients of the damping matrix $[C]$ linked to the nodes placed on the absorbing boundary must be modified according to Eq. (19) [39]. For a 2D problem, Eq. (19) should be added to each node i and each components of the direction, x and y, of the boundary.

$$\begin{aligned} C^{i}_{x} &= m^{i}\rho A_f v^{i}_{x} = m^{i}\rho(L_f e)\left(v_p \cos\alpha_f + v_s \sin\alpha_f\right) \\ C^{i}_{y} &= m^{i}\rho A_f v^{i}_{y} = m^{i}\rho(L_f e)\left(v_p \sin\alpha_f + v_s \cos\alpha_f\right) \end{aligned} \quad (19)$$

where A_f denotes the area of the face of the elements placed in the absorbing boundary (for 2D problems is reduced to the length of the face of the element placed on the boundary, (L_f) multiplied by a thickness (e), normally equal to unity). v^{i}_{x} and v^{i}_{y} are the velocities of the solid phase at the node i in x and y, respectively. α_f is the angle of the absorbing element face with the vertical direction. m^i is a contribution coefficient which considers the participation of each node of the face of the element. For linear-elements (2 nodes by face) $m^i = 1/2$, whereas for quadratic elements (3 nodes by face) $m^i = 1/4$ for the two-external nodes and $m^i = 1/2$ for the internal one. Finally, it must be highlighted that when $\alpha_f = 0°$ (vertical boundary), $v_x = v_p$ and $v_y = v_s$, and vice-versa for horizontal boundaries ($\alpha_f = 90°$).

3.3. Validation examples

The numerical implementation of the ABC detailed above has been checked by 1D-examples for dry soil (solid medium) and saturated soil (two-phase medium). Both examples have been solved considering linear elastic materials without any damping and using the Newmark's method $\gamma = 1/2$, $\beta = 1/4$ and $\theta = 1/2$, when corresponds (free of numerical damping) [36,37], and a time-step equal to 0.01 s. In the dry case, the numerical solution with fixed boundaries and ABC are compared to the analytical solution [40]. For the saturated example, the consolidation of a semi-infinite column is compared for three different length-columns (30 m, 60 m and 100 m) with fixed boundaries and ABC for the shortest one, to compare the behaviour of the reflected waves in different length domains. Details about the geometries, boundary conditions, loading and check points are sketched in Figs. 1 and 2 for dry and saturated cases, respectively. In Fig. 1, a constant (in time) uniformly distributed load is applied on the left side of the bar. The locations of the displacements computed are marked on the bars with a cross and the corresponding distances are sketched (5 m and 15 m from loading sides in figures 1 and 2, respectively). The properties of the materials and the wave velocities are summarized in Tables 1 and 2.

The time histories of the displacement and pore pressure are also plotted in Figs. 1 and 2. For 1D problems, the absorption at the boundary is perfect because the waves incise perpendicularly to the

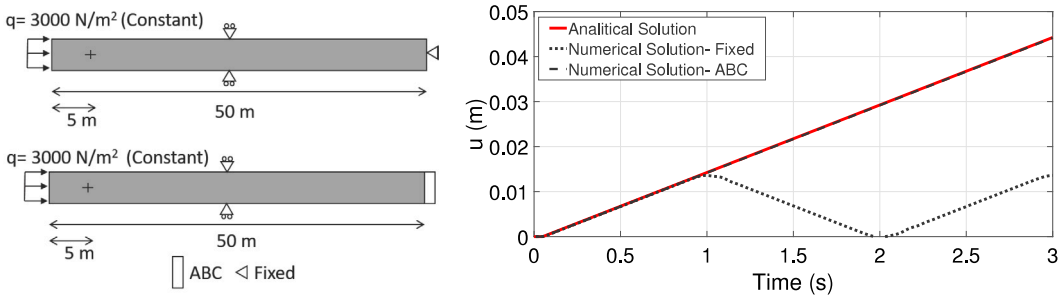

(a) Geometry, boundary conditions and constant uniformly distributed loading

(b) Displacement at $x_i = 5\ m$

Fig. 1. Validation example: dry case (semi-infinite solid bar).

Table 1
Properties of the materials for the validation examples.

Dry case	$\rho = 2000$ kg/m^3	$E = 2 \cdot 10^7$ N/m^2	$\nu = 0$
Saturated case	$\rho_s = 2700$ kg/m^3 $E = 3 \cdot 10^7$ N/m^2 $K_f = 8 \cdot 10^6$ Pa	$\rho_f = 1000$ kg/m^3 $\nu = 0.2$ $k = 1 \cdot 10^{-5}$ m/s	$\rho_{sat} = 1971.43$ kg/m^3 $n = 0.428$

(ρ: density of the dry medium; E: modulus of elasticity; ν: Poisson's ratio; G: shear modulus; K_b: bulk modulus; ρ_s: density of the soil particles; ρ_f: density of the fluid; ρ_{sat}: density of the saturated medium; n: porosity; K_f: bulk modulus of the pore water; k: permeability).

Table 2
Wave velocities to compute the coefficients of damping matrix $[C]$ as Eq. (19) for the validation examples.

Dry case	$v_p = 100$ m/s (Eq. (15)) $v_s = 70.71$ m/s (Eq. (16))
Saturated case	$v_p = 162.41$ m/s (Eq. (17)) $v_s = 79.63$ m/s (Eq. (16))

(v_p: compressive wave velocity; v_s: shear wave velocity).

boundary. The implemented ABC perfectly matches the solution of reference for both problems. In the cases solved with a fixed boundary, artificial oscillations are constantly been reintroduced in the time-history responses because of the reflection of the waves towards the computational domain after impacting on the boundary. These reflected waves invalidate the numerical solution at the control point. In the saturated case, where different lengths of column have been considered, it must be highlighted that the first reflected wave in the response appears at different times, the longer the column, the later it appears, because the wave arrives later to the boundary. By comparing the solution from ABC with respect to the fixed boundary, it can be observed that the ABC solution perfectly matches the fixed solution until the reflected wave appears in each case. Moreover, it can be observed that ABC time histories are kept without any oscillations along the time in consonance with the type of load applied. This example corresponds to a one-dimensional problem, where the waves can only travel in the longitudinal direction of the bar and the viscous-damper is aligned in the bar and the waves direction, therefore the absorption is perfect. It must be pointed out that in the saturated case, the ABC properly works even for the shortest column, and the artificial waves in the displacement and pore pressure responses are out of phase.

4. Numerical investigation of viscous dampers-ABC

Plenty of artificial waves are reintroduced into the computational domain because the fixed boundaries act like sources of new waves. The time-responses can be chaotic because multiple waves (both original and reflected waves) are superposed, and therefore, the improvement achieved by the ABC cannot be easily evaluated. For viscous-dampers ABC, the main interest has been focused on the arrival of the waves on the boundary, highlighting that the angle of incidence determines the possible reflected waves. However, attention should also be paid to how the resulting waves are approaching towards the area of interest, which is normally farther from the boundaries. Complex processes of interaction and transformation between waves can occur during the propagation of the waves in the medium.

In this section, the position (distance and orientation) of the fixed boundaries and the influence of the viscous damper-ABC are analysed from a signal processing framework by means of several robust numerical schemes which are mainly supported on the spectral properties and energy content of the response. According to this framework, each time-history response, computed from a time-domain FEM, is analysed like a signal. An exhaustive numerical analysis has been carried out for plane strain problems, in both dry and saturated soil.

4.1. Description of the numerical model

The numerical model developed in this research is defined by four computational domain sizes, which are progressively incremented, as is sketched in Fig. 3. It is well-known that the larger the computational domain, the less artificial waves in the domain because of the fixed boundaries. Similar considerations have been also employed by other researchers [11,41]. The model corresponds to a square region with symmetry condition on the left-vertical boundary, the ground surface is the upper boundary, and the rest of the boundaries represent the outgoing medium. The sizes considered are 10 × 10 m (M1010), 20 × 20 m (M2020), 35 × 35 m (M3535) with both fixed and ABC conditions, and 50 × 50 m (M5050) with ABC condition for reference solution. For preventing uncertainties in the comparative study, the following numerical parameters have been adopted for all the models.

A regular mesh with 0.5 × 0.5 m quadrilateral elements of 4-nodes has been used. The horizontal displacements of the left boundary

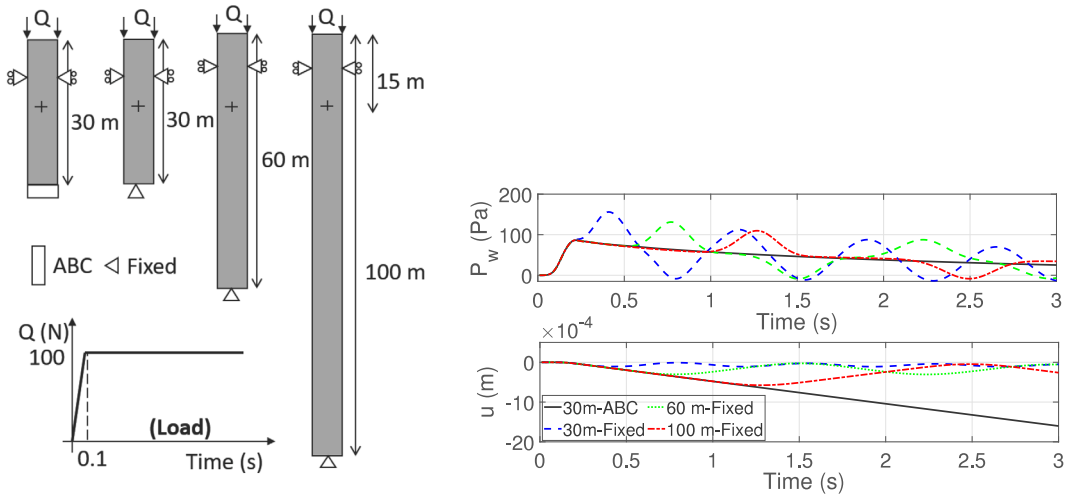

(a) Geometry, boundary conditions and loading

(b) Displacement and pore pressure at $y_i = 15\ m$

Fig. 2. Validation example: saturated case (semi-infinite saturated soil column).

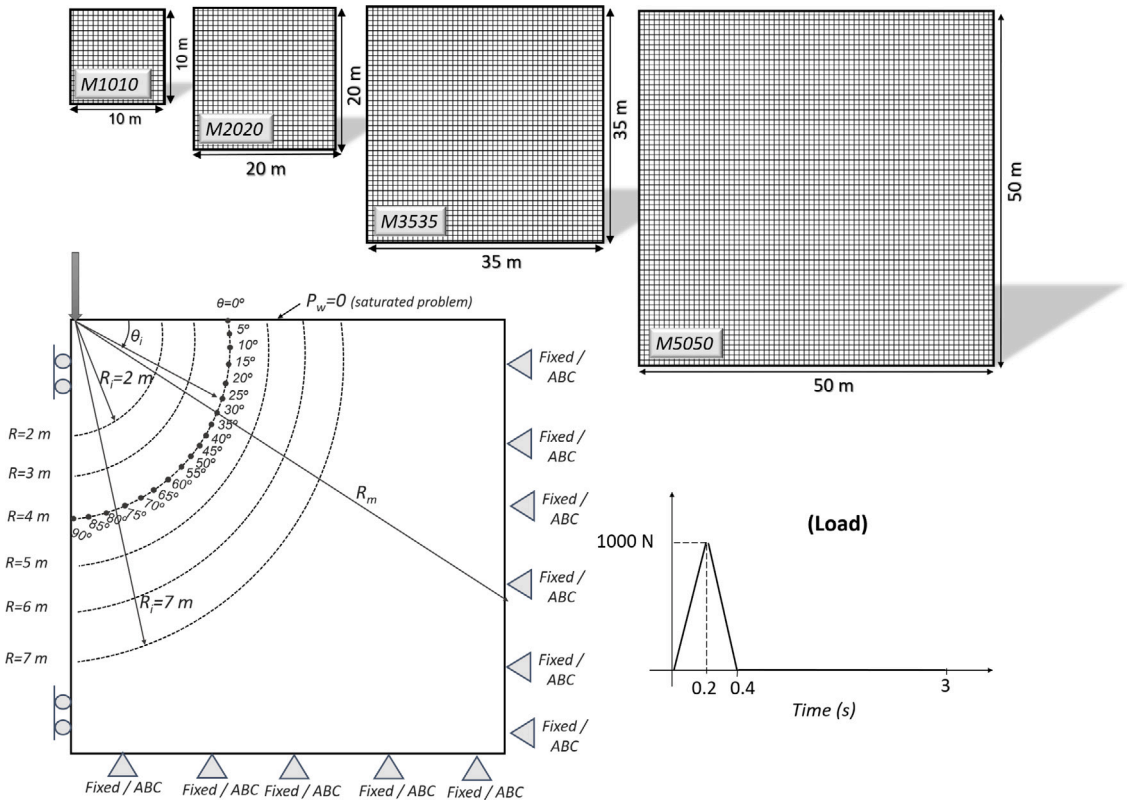

Fig. 3. Computational domain sizes, boundary conditions, loading and check points (R_i, θ_i, R_m).

(symmetry) are restricted while the lower and right boundaries, fixed or ABC are imposed depending on the case. For the saturated models, null pore water pressure condition is imposed on the ground.

A punctual down-vertical triangular load, with amplitude and duration equal to 1000 N and 0.4 s (2.5 Hz), respectively, is applied on the left node on ground-surface, Fig. 3. This simple load has been used to excite the system with the aim of highlighting properly the frequency-content linked exclusively to the artificial waves after reflecting on the boundaries or their absence in the ABC solutions. Other complex loading cases cannot be considered to prevent the mixture of frequencies between the response to the input load and the reflected waves. According to the literature [8,11], the response of viscous dampers does not depend on the frequency content of the input load. Therefore, it can be asserted that the waves which are propagating in the medium are due exclusively to the free-vibration of the system and the reflected waves.

Table 3
Material properties for the numerical model.

Dry case	$\rho = 2000$ kg/m^3	$E = 6.67 \cdot 10^7$ N/m^2	$\nu = 0.25$
Saturated case	$\rho_s = 2700$ kg/m^3 $E = 6.67 \cdot 10^7$ N/m^2 $K_f = 8 \cdot 10^6$ Pa	$\rho_f = 1000$ kg/m^3 $\nu = 0.25$ $k = 1 \cdot 10^{-5}$ m/s	$\rho_{sat} = 2000$ kg/m^3 $n = 0.412$

(ρ: density of the dry medium; E: modulus of elasticity; ν: Poisson's ratio; G: shear modulus; K_b: bulk modulus; ρ_s: density of the soil particles; ρ_f: density of the fluid; ρ_{sat}: density of the saturated medium; n: porosity; K_f: bulk modulus of the pore water; k: permeability).

Table 4
Wave velocities to compute the coefficients of damping matrix [C] as Eq. (19) for the numerical model.

Dry case	$v_p = 200$ m/s (Eq. (15)) $v_s = 115.5$ m/s (Eq. (16))
Saturated case	$v_p = 223$ m/s (Eq. (17)) $v_s = 115.5$ m/s (Eq. (16))

(v_p: compressive wave velocity; v_s: shear wave velocity).

Neither material damping or numerical damping are included in this numerical experiment, in order to prevent other sources of dissipation or attenuation of the waves, except by the ABC. Therefore, linear elastic isotropic material is considered, which corresponds to the most unfavourable model to analyse the ABC behaviour. The properties of the material and wave velocities are listed in Tables 3 and 4, where similar p and s-wave velocities are used in both types of problems. Moreover, the Newmark's integration algorithm $\gamma = 1/2$ $\beta = 1/4$, $\theta = 1/2$ (free of numerical damping) has been chosen, and a time-step $\Delta t = 0.005$ s, which allows to analyse high-frequency components, up to 100 Hz according to Nyquist frequency criterion. The computation of each case has been maintained during 3 s to assure that an enough amount of reflected waves takes place.

A dense radial grid of check points has been monitored to track the transformation of the time-responses when approaching to the area of interest, which has been established close to the point of loading. For that, six concentric distances (named as radius R_i) measured from the loading point, have been defined from $R_1 = 2$ m to $R_6 = 7$ m, with increment equal to 1 m. For each radius, nineteen angles (θ_i) have been established to consider the influence of the orientation of the boundaries in the resulting signal registered in each point. These angles are defined by increments of 15° in clockwise direction, from $\theta_1 = 0°$ (ground surface) to $\theta_{19} = 90°$ (symmetry boundary), as shown in Fig. 3.

This analysis has been developed for displacement, stress and pore pressure (saturated case only) time-history responses, since the influence of the boundaries on each variable is unknown in advance and should be investigated. The following nomenclature is used herein: u_h and u_v are the horizontal and vertical displacements, respectively; σ_h, σ_v and τ are the horizontal, vertical and shear stresses, respectively; and p_w is the pore pressure. As reference, the computational costs of each domain respect to the smallest one (M1010), measure in terms of computational time, are 2.4, 19, 232.4 times higher for M2020, M3535 and M5050, respectively. Very Slight differences in terms of computational cost have been observed between fixed and ABC models.

4.2. Time-history and frequency response

For comparison purposes and the sake of briefness, the time-histories u_h, σ_v and power p_w have been monitored at $R = 2$ m-$\theta = 45°$ as representative examples. The corresponding frequency response spectra are also included, which are supported on the amplitude and unwrapped phase response spectra computed by the Fourier transform (rectangular window) of each time-history. They can reveal the frequency-content of each signal highlighting the amount of waves travelling in the medium. Amplitude spectra denotes the contribution of each frequency (wave) to the overall response, whereas phase spectra represents the alignment of the waves in time.

Figs. 4 (dry problem) and 5 (saturated problem) show the responses obtained with ABC and fixed boundary conditions for the four computational domain sizes. In both cases, plenty of oscillations (reflected waves) due to the fixed boundary can observed, which are more relevant for the results of displacements and pore pressures. For each domain, the reflected waves are highlighted in the amplitude spectra by means of peaks associated to the different frequencies. On the contrary, the ABC solutions present smoothed patterns with lower amplitudes, and good agreement between the two largest computational domain sizes investigated. In the case of the fixed boundary solutions, the shorter computational domain size, the higher increment of the amount of waves in the response, namely, more peaks of great amplitude associated to higher frequencies. Moreover, the fixed-responses for the different computational sizes are out of phase, whereas ABC-solutions are in-phase since their phase spectra are constantly linear almost the whole range of frequencies, and in general they also coincide for most of the domains, especially for σ_v. This suitable alignment between phase-spectra for different domains reveals that the waves in the medium are well-organized, reducing the interaction between them and the cluttered time responses.

4.3. Directional spectra

Directional spectra display information on the distribution of the amplitude spectra and frequency-content of each time-history according to the direction θ. The influence of the boundaries, distance and orientation, can be analysed on each variable inside the region of interest. Firstly, the improvement achieved with ABC versus fixed boundaries has been plotted in Figs. 6 (dry problem) and 7 (saturated problem) for the computational domain M3535 and the closest radius to the boundaries, $R = 7$ m. The frequency axis has been trimmed down for improving the compression of the graphs. In these figures, it can be observed that the ABC have significantly smoothed the spectra, removing ripples and peaks in the whole range of frequencies and directions, and reducing the amplitude for all the variables investigated respect to the fixed solutions. The general trend between ABC and fixed solutions matches for u_v, σ_v, τ and P_w but a higher disagreement is observed for the lower values of θ in u_h and the lower and upper values of θ in σ_h, far from the ground surface, so the horizontal responses can be affected by the fixed boundaries. It must be pointed out that the range of frequencies, the amplitude of which is significant, varies for each variable. A wider range of frequencies is observed in the stress than in the displacement or pore pressure time-histories, although slight differences can also be observed between horizontal and vertical displacements.

Secondly, in order to assess the influence of the enlargement of the domain, the directional spectra for the four computational sizes with ABC at $R = 7$ m have been compared in Figs. 8 (dry problem) and 9 (saturated problem). For all variables, the spectra corresponding to M3535 and M5050 properly match, M1010 presents the most discrepant pattern in all cases, whereas M2020 is closer to the larger domains in stress and pore pressure responses and further for displacements. Therefore,

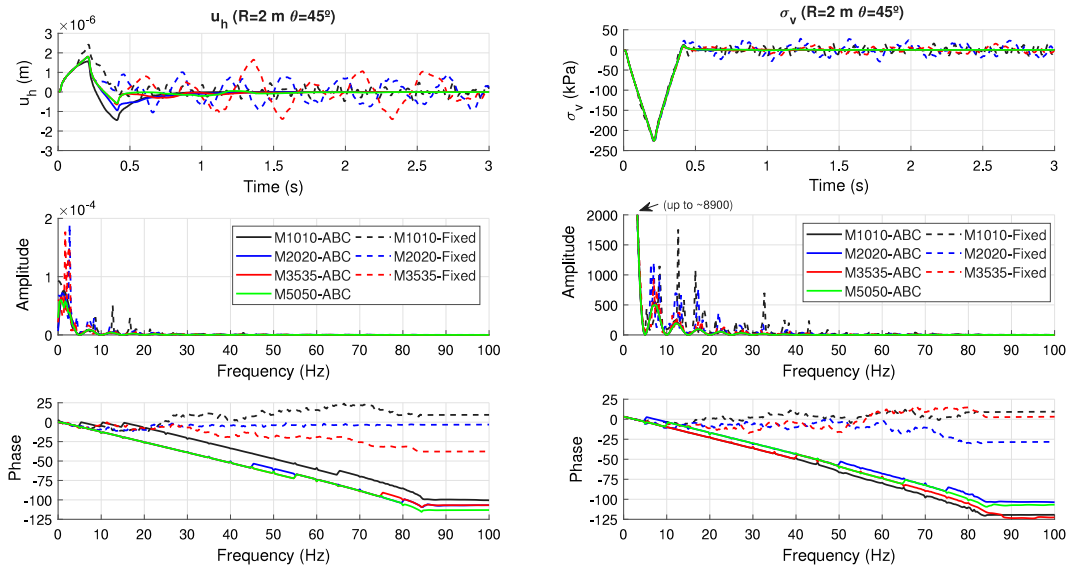

Fig. 4. Dry problem: time-history responses and frequency spectra at $R = 2m - \theta = 45°$.

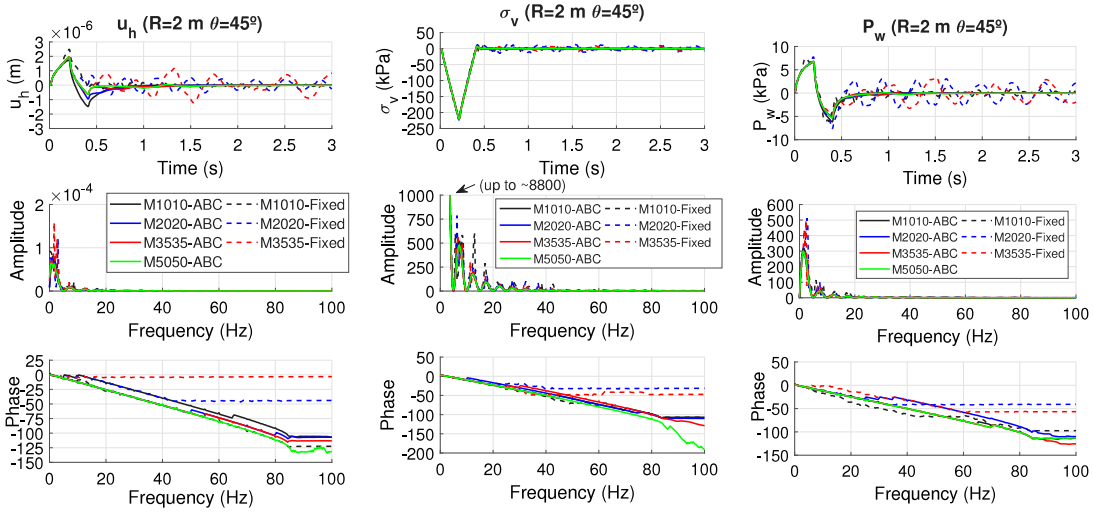

Fig. 5. Saturated problem: time-history responses and frequency spectra at $R = 2m - \theta = 45°$.

M5050-ABC can be suitable used as reference solution for comparison purposes. According to the previous comparison, the length of the range of relevant frequencies that affects more each signal (time-history) varies for each variable, but it is independent of the computational domain size for ABC solutions.

4.4. Energy approach: Parseval's relation

In the literature, the verification of the suitable behaviour of a viscous dampers ABC is normally simplified to the comparison of some particular time-histories responses. However, in this research an energy approach, supported on the Parseval's relation, is proposed to evaluate the viscous dampers ABC. The time and frequency representations of a signal are equivalent, and therefore the Parseval's relation establishes that a time-domain signal and its corresponding frequency-domain representation must have the same energy content [42]. From a discrete Fourier transform, this relationship can be defined as Eq. (20), which asserts that the total energy (E_t) of a time signal $x(t)$ is equal to the total energy of its discrete Fourier transform $X(f)$ along the whole range of frequencies, where t and f are the time and frequency, respectively, and N the number of individual samples in the signal.

$$E_t = \sum_{t=0}^{N-1} |x(t)|^2 = \frac{1}{N} \sum_{f=0}^{N/2} |X(f)|^2 \tag{20}$$

The relative energy error of each time-history has been defined with respect to the solution of reference (M5050-ABC) and has been plotted in Figs. 10 and 11 for dry and saturated problems, respectively. The energy error is expressed with respect to the length $R_m - R_i$, which corresponds to the shortest path for the arrival of the reflected waves to each checkpoint. R_i represents the distance between the point-load and the check-point and R_m is the length between the point-load and the nearest boundary passing by this particular check-point, as shown in Fig. 3. The lower the values of $R_m - R_i$, the closer a boundary to the checkpoint is, independently of θ. ABC and fixed boundary conditions and the computational sizes M1010, M2020 and M3535 are analysed for all the variables.

The errors for ABC, in terms of energy content in the signal (time-history) are significantly lower than for the fixed boundary conditions, excluding u_v computed with M1010 and M2020. In these two particular cases, the fixed-solutions present an anomalous behaviour due to the shortness of the computational domain, since the reflected waves

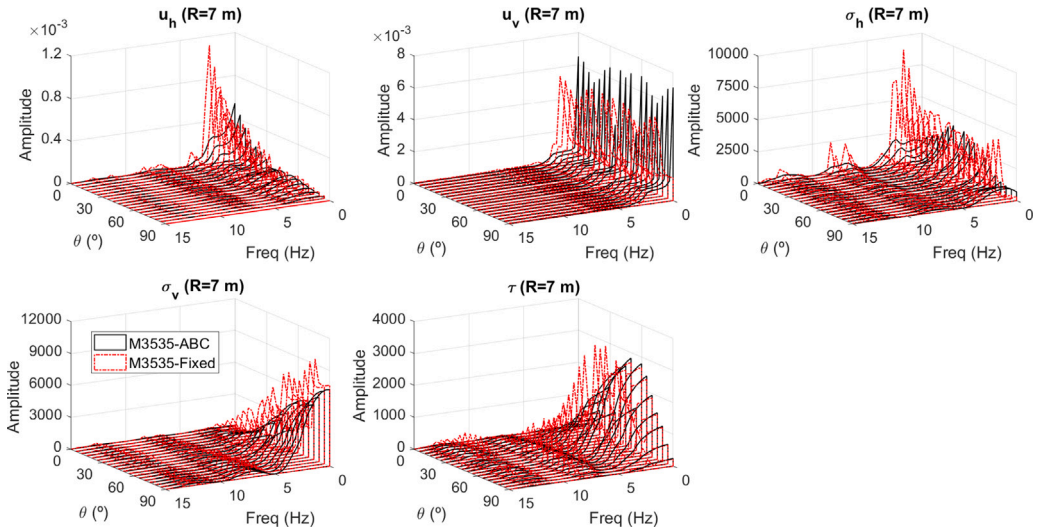

Fig. 6. Dry problem: comparison of directional spectra at $R = 7$ m for M3535 computed with ABC and fixed boundary conditions.

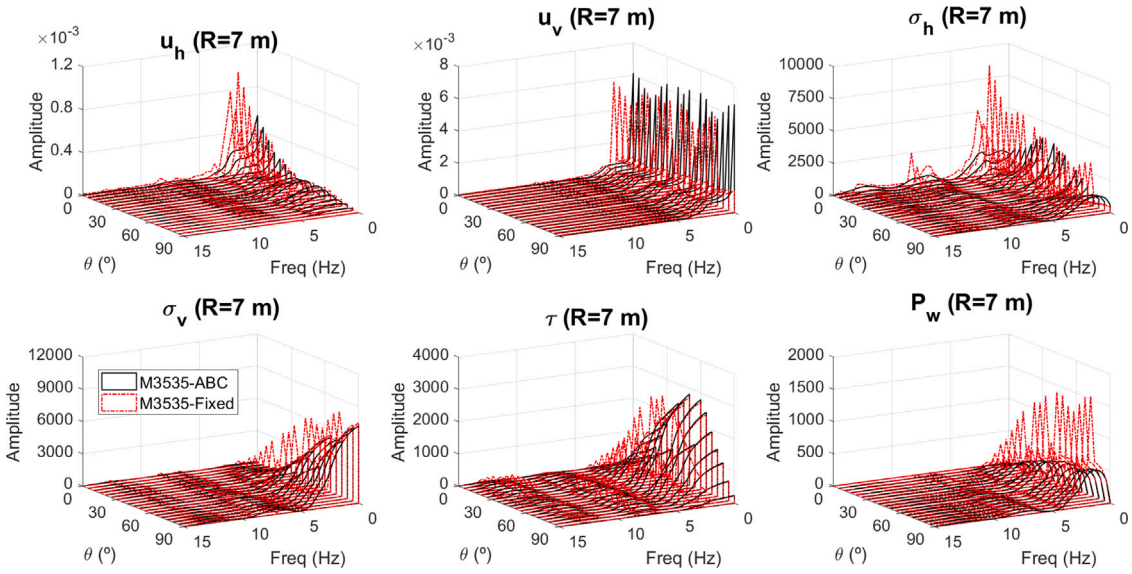

Fig. 7. Saturated problem: comparison of directional spectra at $R = 7$ m for M3535 computed with ABC and fixed boundary conditios.

disturb the time-history responses from the beginning, obtaining almost null values of u_v, and therefore almost null values of energy, which is unrealistic. Surprisingly, in the case of u_h and σ_h computed with fixed conditions, the larger the computational domain, the greater the energy error, which are also consistent with the time-histories and frequency spectra in Figs. 4 and 5 (case of u_h). Probably, this reveals that the chaotic swarm of waves travelling in the media can be re-organized attending to its frequency content as the computational domain is larger, which seems to be more relevant for horizontal variables than for the others. Therefore, for fixed solutions, the relative energy error does not always improve for larger computational domains. For all the variables in the ABC solutions, both magnitude and dispersion of the errors are significantly reduced in a staggered manner as the computational domain size is increased. In the case of M3535, the error tends to be constant and independent of the distance to any boundaries ($R_m - R_i$) in all the variables, achieving a relative energy error lower than 0.5%. In the case of M2020, the dispersion of the error is slightly higher, but lower than ≈2%. Hence it can be stated that an enlargement from M3535 to M5050, computed with ABC, does not introduce an improvement in the accuracy of the responses. Moreover, despite the reflected waves in the boundaries presenting multiple angles of incidence, the influence on the time-history response in the area of interest is negligible.

4.5. Bandwidth

The bandwidth is an spectral property that defines the range of frequencies in which the energy of a signal is contained. By means of the bandwidth parameter, the effect of the boundaries over the frequency components of each signal is investigated. To highlight the whole range of frequencies that appears in the signal, the occupied bandwidth for a threshold of the 99% of the energy is established. It has been observed that the lowest frequency is similar in all the cases, nearly null, and therefore the widest values of bandwidth have been considered regardless the check point position. For each variable and computational domain, the relative energy error ($Error^E$) and the relative bandwidth errors ($Error^{Bw}$) with respect to the reference solution (M5050ABC) have been listed in the Table 5, for both types of problems and boundary conditions. From this table, it can be observed that the bandwidth errors for the fixed problems are significantly higher than ABC, which implies that the bandwidth for ABC is narrower because of the reduction of the frequency-content, especially the high-frequencies,

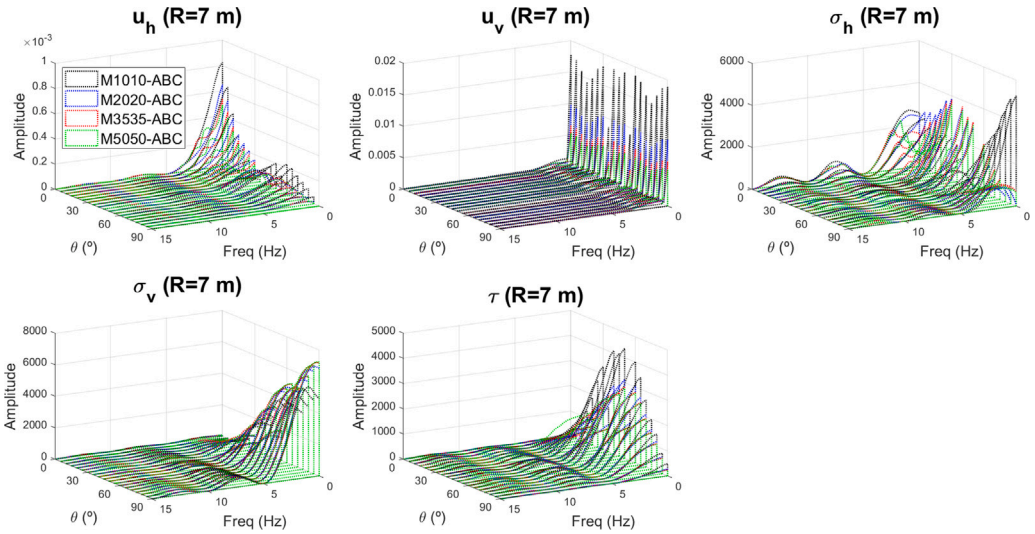

Fig. 8. Dry problem: comparison of directional spectra at $R = 7$ m for the four computational domain sizes with ABC.

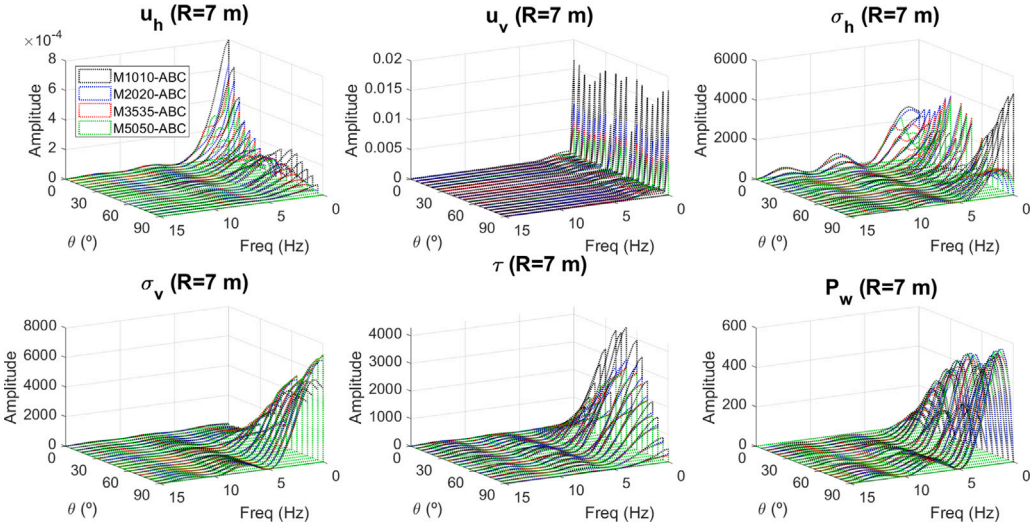

Fig. 9. Saturated problem: comparison of directional spectra at $R = 7$ m for the four computational domain sizes with ABC.

because they avoid artificial waves thanks to the viscous-dampers. On the other hand, a slight influence of the computational domain size can be observed on the relative bandwidth errors between ABC solutions, whereas it has a more relevant influence on the energy errors, as exposed above. Therefore, it can be concluded that, for ABC, an enlargement of the computational size slightly affects to the bandwidth, namely the frequency content and high-frequencies, but it reduces the artificial energy content of the signal.

4.6. Spectral coherence

For statistical signal processing and time-series analyses, the spectral coherence is an statistic that compares two signals and indicates how well one signal corresponds to the other one at each frequency, measuring the linear correlation between them [43]. The coherence (C_{xy}) between two signals x and y depends on frequency and it is calculated from Eq. (21), where P_{xx} and P_{yy} are the power spectral densities of the x-signal and y-signal, respectively, and P_{xy} is the cross power spectral density. Spectral coherence varies between 0 and 1, and when two signals are exactly identical, the coherence is equal to 1. Therefore, the higher the coherence, the greater the similarity between the two analysed signals.

$$C_{xy} = \frac{|P_{xy}|^2}{P_{xx}P_{yy}} \tag{21}$$

To investigate the influence of the enlargement of the computational domain and the corresponding reduction in the energy error highlighted above depending on the frequency, the spectral coherence is estimated for ABC solutions, comparing the computational domains M1010, M2020 and M3535 with respect to M5050. The values are plotted in Figs. 12 and 13 for dry and saturated cases, respectively, and for all the check-points located at $R = 7$ m, which is the nearest distance to the boundaries.

As expected, the lowest values of coherence can be found for M1010, in a wider range of θ and frequencies, for most of the analysed variables. Comparing M2020 and M3535, the shape-patterns of the spectral coherence along θ and frequency are very similar. This behaviour supports the discussion previously outlined for ABC, since despite of the enlargement of the computational domain, the range of frequencies is not significantly altered. The coherence in M3535 with respect to M2020 slightly improves for the stresses and pore pressure,

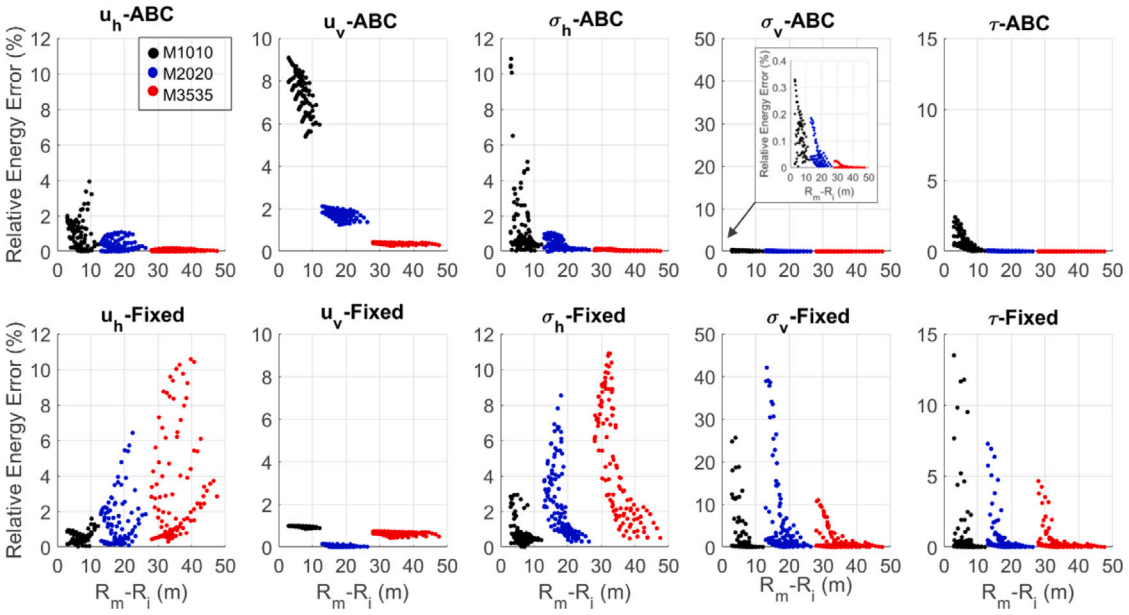

Fig. 10. Dry problem: relative energy error of each time-history.

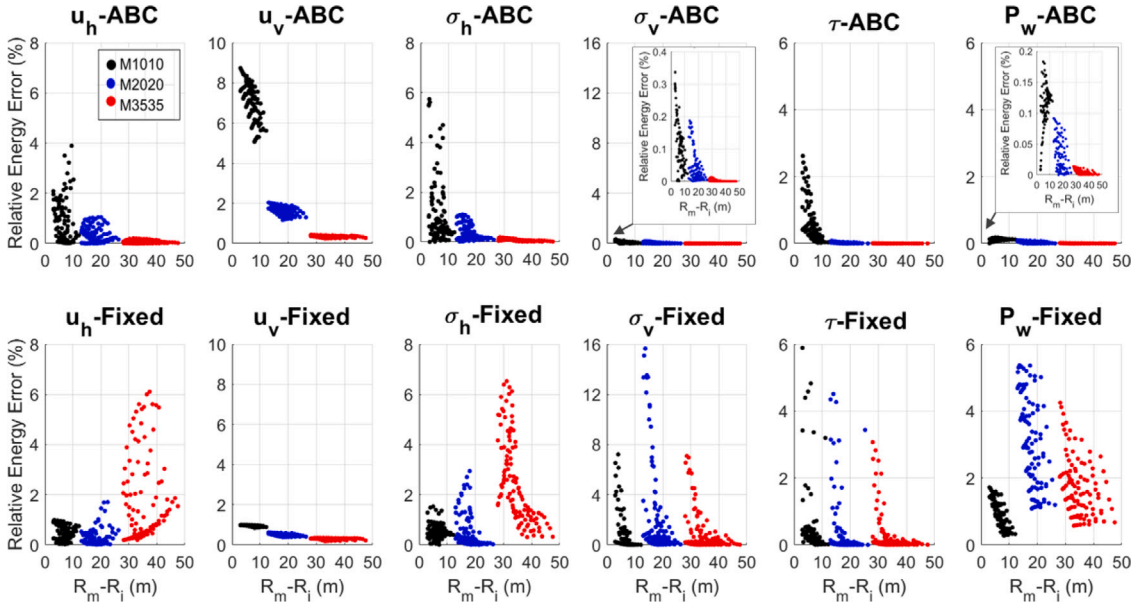

Fig. 11. Saturated problem: relative energy error of each time-history.

and moderately does so for the displacement too. In both cases, the spectral coherence of the stress responses are significantly lower than 1 for the upper range of frequencies and the extremal values of θ, which indicate locations mainly close to the ground surface and to the symmetry boundary. However, the coherence obtained for the pore pressure is close to 1 except for the higher frequencies, regardless θ. For the vertical displacement, the coherence is fairly uniform, independently of θ and frequency, closer to 1 as the domain is larger, whereas for the horizontal displacements, the coherence is significantly lower than 1 for a range of frequencies and θ wider than the rest of variables.

For most of the variables, lower values of coherence are observed for high-frequencies, and therefore the reduction in the energy error due to the enlargement of the computational domain observed previously, affects mainly to this range of high-frequencies. Since the range of high frequencies is normally out of practical interest, the obtained results with ABC are suitable, since the coherence approaches 1 in the range of frequencies of practical interest.

5. Conclusions

A signal processing approach has been applied to analyse the behaviour of the viscous-damper ABC in time-domain FEM. Each time-history is treated like a signal, attending to its frequency and energy content and spectral properties. ABC has been investigated in dry media and saturated problems, with a $u - p_w$ formulation modifying the velocity of the first longitudinal wave considering only the fluid bulk modulus [9]. For comparison purposes, both ABC and fixed boundary conditions have been investigated by means of a numerical model without material or numerical damping, monitoring displacements, stresses and pore pressure along a dense spatial grid of check points.

Table 5
Relative energy (E) and bandwidth (Bw) errors.

Variable	Size	Dry case				Saturated case			
		$Error^{E}$ (%)		$Error^{Bw}$ (%)		$Error^{E}$ (%)		$Error^{Bw}$ (%)	
		ABC	Fixed	ABC	Fixed	ABC	Fixed	ABC	Fixed
u_h	M1010	3.93	1.59	0.58	6.34	3.90	0.99	0.6	6.4
	M2020	1.09	6.42	0.46	2.19	1.05	1.7	0.46	2.13
	M3535	0.19	10.57	0.22	1.32	0.21	6.11	0.28	1.75
u_v	M1010[a]	9.08	0.99	0.21	6.87	8.74	1	0.2	5.06
	M2020[a]	2.11	0.15	0.08	0.61	2.04	0.62	0.08	1.08
	M3535	0.44	0.74	0.03	0.71	0.43	0.35	0.03	1.33
σ_h	M1010	10.84	2.93	0.98	11.77	5.74	1.53	1.39	6.82
	M2020	1.05	8.52	0.49	3.8	1.11	2.94	0.51	4.07
	M3535	0.15	10.89	0.38	1.24	0.19	6.52	0.39	2.31
σ_v	M1010	0.33	25.59	0.8	7.58	0.34	7.21	3.02	6.37
	M2020	0.19	42.07	0.49	3.1	0.18	15.66	3.07	3.09
	M3535	0.03	10.99	0.07	2.16	0.012	7.08	3.03	3.12
τ	M1010	2.4	13.48	0.39	8.67	2.62	5.89	1.07	8.88
	M2020	0.046	7.26	0.80	7.87	0.08	4.51	1.05	7.81
	M3535	0.006	4.63	0.81	6.78	0.008	3.48	1.01	7.05
P_w	M1010	–	–	–	–	0.18	1.72	0.74	4.82
	M2020	–	–	–	–	0.09	5.37	0.29	1.32
	M3535	–	–	–	–	0.014	4.25	0.2	1.29

[a]Anomalous behaviour exposed above.

The scope of this research is focused on the characterization of time-history responses close to the area of interest, alternatively to the traditional approach about the angle of incidence on the boundaries, by means of a digital signal processing approach. Especial attention has been paid to the size of the computational domain, which is a crucial task in this matter, from both accuracy and computational-cost points of view. For saturated porous media, the modification of p-wave proposed is suitable according to the validation examples. The main conclusions are listed below.

– The influence of ABC or fixed boundary conditions is not homogeneous for all variables, being the vertical displacement the least sensible to the ABC.

– Numerous reflected waves due to the fixed boundaries have been highlighted by the spectral characterization of the signals. For the shortest computational domain, a high amount of reflected waves with great amplitude, linked to higher frequencies, are observed. Whereas for ABC solutions, smoother spectral patterns with lower amplitude and without ripples or peaks have been obtained.

– ABC solutions are in-phase thanks to the reduction of the frequency content of the signal after ABC, but not in fixed conditions.

– For ABC solutions, the spectral characterization of M3535 and M5050 is quite in agreement between dry and saturated problems. The shortest domain (M1010) presents striking differences in the spectral patterns in most of the cases, whereas the intermediate size (M2020) approaches the larger domains in stress and pore pressure responses but not in displacement. For fixed boundaries, the solution does not always improve with the increment of the domain.

– The estimated energy errors of the signals for ABC are significantly lower in most of the variables respect to the corresponding fixed solutions. In general, the larger computational domain, the lower energy error for ABC. Inside the area of interest, the energy error is lower than 2% in M2020 and 0.5% in M3535, which tends to be independent of the distance and the angles of incidence on the boundaries. An enlargement from M3535 to M5050 is not worth it.

– The range of frequencies is wider for stress than pore pressure and displacements. The bandwidth is considerably wider for fixed solutions than for ABC, where the high-frequency content is removed. The influence of the enlargement of the computational domain on the bandwidth of ABC is not significant. The spectral coherence also supports these findings, since M1010 presents the lowest values of coherence for a wider range of orientations, frequencies and variables, whereas M2020 and M3535 are similar. The spectral coherence depends on each variable being the vertical displacement the least sensible to the frequency content and boundary orientation. The lowest values of coherence correspond to high-frequencies, hence the enlargement of the computational domain reduces the energy of those waves associated to high-frequency.

It is worth to highlight that, in a practical application of this research, there is no need to repeat the same analysis as have been conducted in the present research, as the previously listed conclusions will be valid. Therefore, this research presents results of direct and practical application in the numerical analysis of soil dynamic problems. Some general user's guidelines can be outlined: viscous-dampers ABC (VD-ABC) can be confidently used with intermediate sizes of domain of computation. Small domains should be avoided since errors are still relevant despite ABC, whereas it is not worth to use large or huge domains since the accuracy does not significantly improve but so does the computational cost. For a tentative approximation of the computational domain, it is recommended to compare the time-histories responses of several variables between two possible sizes, and in particular, the comparison of only vertical displacements is not recommended. Finally, if any damping source (material or numerical) is included in the model, the behaviour of VD-ABC will enhance respect to the findings observed in this research. Not specific considerations should be taken into account between dry and saturated problems.

CRediT authorship contribution statement

Juana Arias-Trujillo: Conceptualization, Methodology, Software, Formal analysis, Writing – original draft, Writing – review & editing. **Susana López-Querol:** Software, Resources, Writing – review & editing, Supervision.

Declaration of competing interest

The authors declare that they have no known competing financial interests or personal relationships that could have appeared to influence the work reported in this paper.

Data availability

Data will be made available on request.

Acknowledgements

The academic numerical finite element code GeHoMadrid has been used to implement the numerical scheme described. The authors want to express their gratitude to Prof. Manuel Pastor for the kind availability of the code. The authors also deeply appreciate the continuous support provided by Prof. Rafael Blaquez during this research. The first author wants to thank the financial support provided by the Spanish Ministry of Science and Innovation (scholarship BES-2008-002770) during the very preliminary stage of this research, and the Consejeria de Economia, Ciencia *y* Agenda Digital de la Junta de Extremadura and the European Regional Development Fund of the European Union through the reference grant GR21143, for concluding this research.

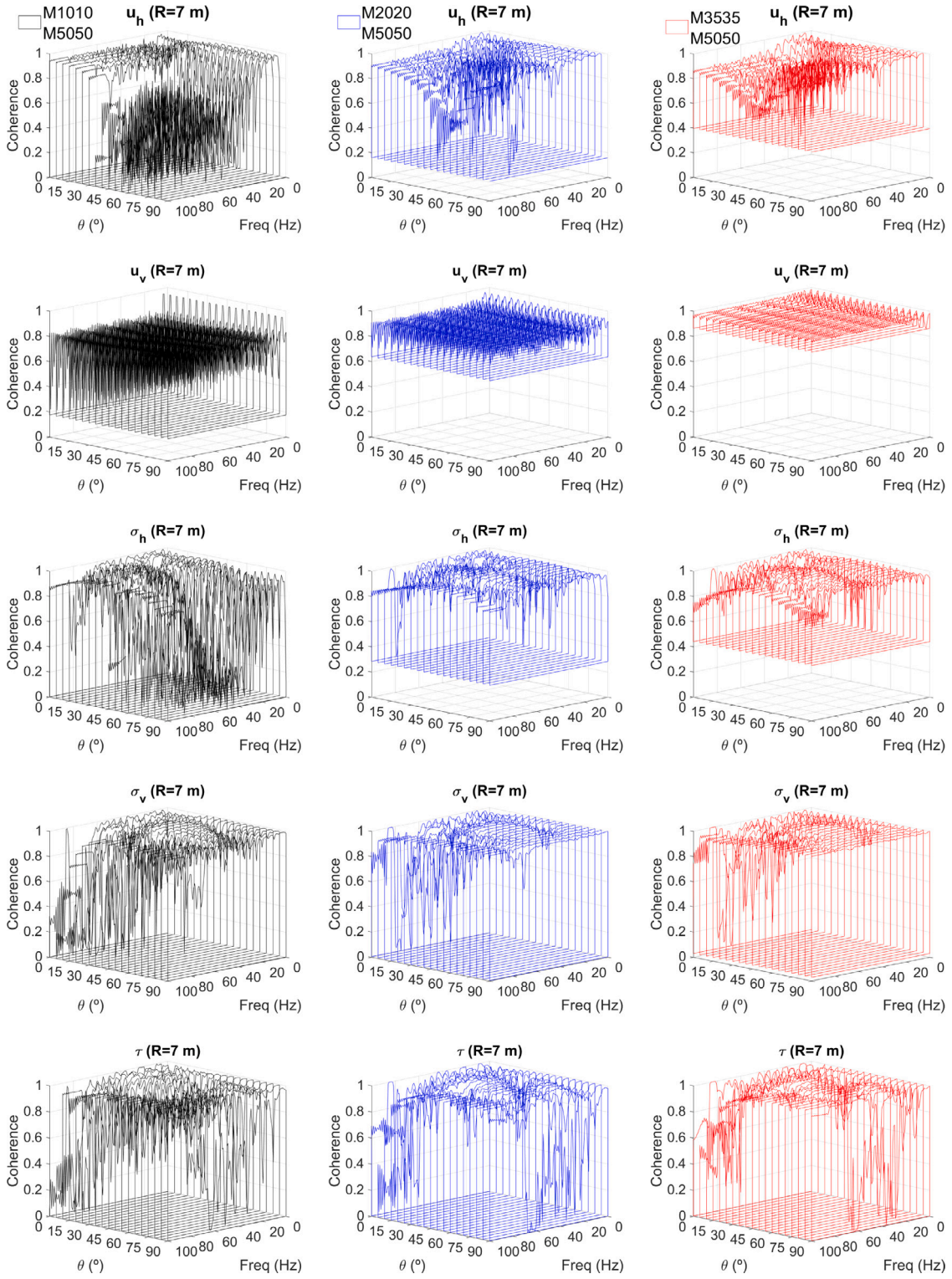

Fig. 12. Dry problem: spectral coherence for ABC solutions between M1010, M2020 and M3535 respect to M5050.

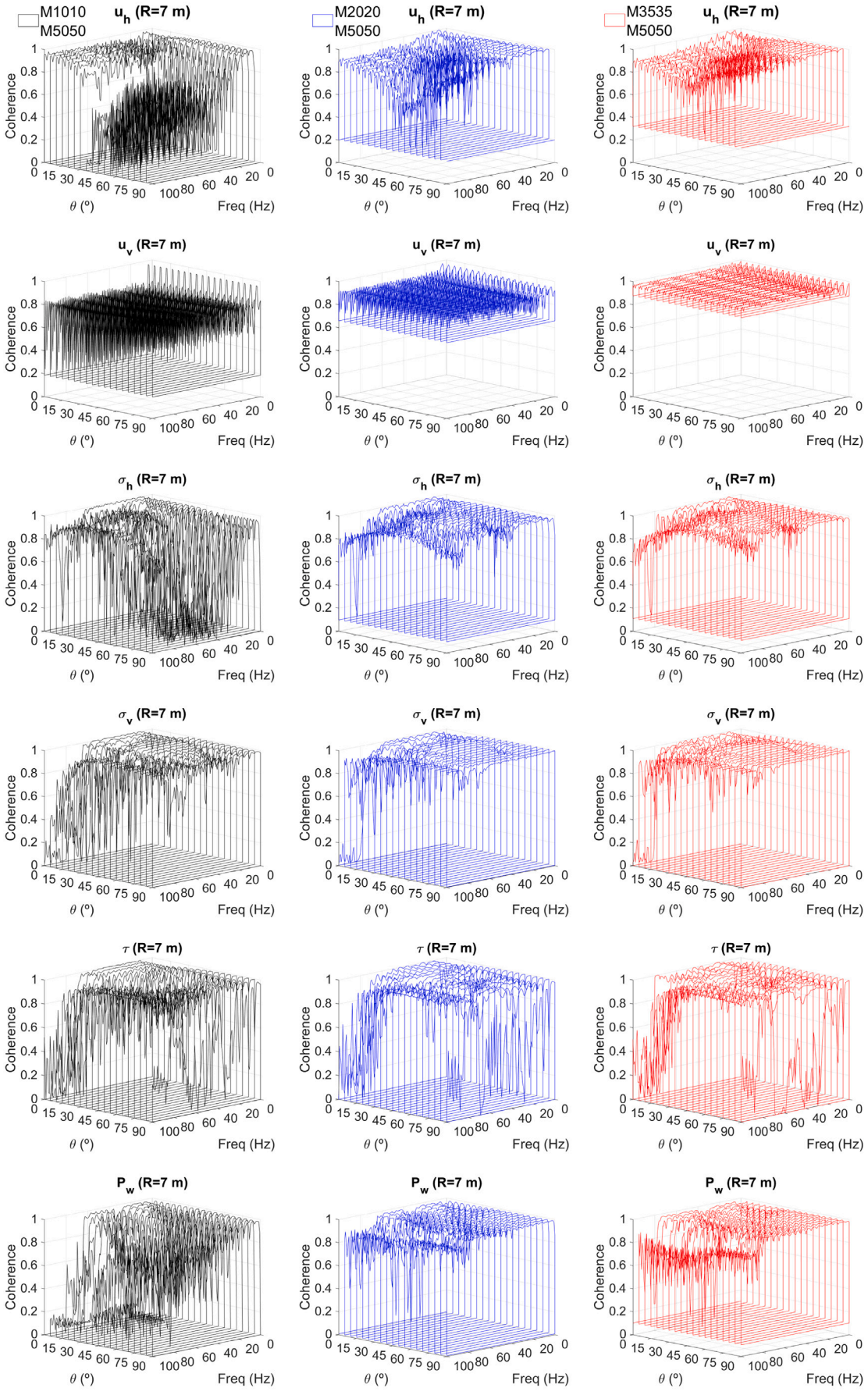

Fig. 13. Saturated problem: spectral coherence for ABC solutions between M1010, M2020 and M3535 respect to M5050.

References

[1] Kontoe S, Zdravkovic L, Potts DM. An assessment of the domain reduction method as an advanced boundary condition and some pitfalls in the use of conventional absorbing boundaries. Int J Numer Anal Methods Geomech 2009;33(3):309–30.

[2] Duhamel D, Nguyen TM. Finite element computation of absorbing boundary conditions for time-harmonic wave problems. Comput Methods Appl Mech Engrg 2009;198:3006–19.

[3] Semblat JF, Lenti L, Gandomzadeh A. A simple multi-directional absorbing layer method to simulate elastic wave propagation in unbounded domains. Internat J Numer Methods Engrg 2011;85(12):1543–63.

[4] Li P, Song EX. A viscous-spring transmitting boundary for cylindrical wave propagation in saturated poroelastic media. Soil Dyn Earthq Eng 2014;65:269–83.

[5] Li P, Song EX. A general viscous-spring transmitting boundary for dynamic analysis of saturated poroelastic media. Int J Numer Anal Methods Geomech 2016;40(3):344–66.

[6] Shi L, Wang P, Y. Cai Y, Cao Z. Multi-transmitting formula for finite element modeling of wave propagation in a saturated poroelastic medium. Soil Dyn Earthq Eng 2016;80:11–24.

[7] Xu C, Song J, Du X, Zhao M. A local artificial-boundary condition for simulating transient wave radiation in fluid-saturated porous media of infinite domains. Internat J Numer Methods Engrg 2017;112(6):529–52.

[8] Lysmer J, Kuhlemeyer RL. Finite dynamic model for infinite media. J Eng Mech Div ASCE 1969;95(4):859–77.

[9] Yang J. Pore pressure coefficient for soil and rock and its relation to compressional wave velocity. Geotechnique 2005;55(3):251–6.

[10] Kramer SL. Geotechnical earthquake engineering. Englewood Cliffs, NJ: Prentice-Hall; 1996.

[11] Kontoe S. Development of time integration schemes and advanced boundary conditions for dynamic geotechnical analysis [Ph.D. thesis], London, United Kingdom: Department of Civil and Environmental Engineering. Imperial College of Science, Technology and Medicine; 2006.

[12] Al-Homoud AS, Whitman RV. Seismic analysis and design of rigid bridge abutments considering rotation and sliding incorporating non-linear soil behavior. Soils Dyn Earthq Eng 1999;18:247–77.

[13] Smith WD. A nonreflecting plane boundary for wave propagation problems. J Comput Phys 1974;15(4):492–503.

[14] Clayton R, Engquist B. Absorbing boundary conditions for acoustic and elastic wave equations. Bull Seismol Soc Am 1977;67(6):1529–40.

[15] Liao ZP, Wong HL. A transmitting boundary for the numerical simulation of elastic wave propagation. Int J Soil Dyn Earthq Eng 1984;3(4):174–83.

[16] Higdon RL. Radiation boundary conditions for elastic wave propagation. SIAM J Numer Anal 1990;27(4):831–69.

[17] Givoli D. High-order nonreflecting boundary conditions without high-order derivatives. J Comput Phys 2001;170:849–70.

[18] Givoli D, Hagstrom T, Patlashenko I. Finite element formulation with high-order absorbing boundary conditions for time-dependent waves. Comput Methods Appl Mech Engrg 2006;195:3666–90.

[19] Hagstrom T, Mar-Or A, Givoli D. High-order local absorbing conditions for the wave equation: Extensions and improvements. J Comput Phys 2008;227:3322–57.

[20] Rabinovich D, Givoli D, Bielak J, Hagstrom T. A finite element scheme with a high order absorbing bondary condition for elastodynamics. Comput Methods Appl Mech Engrg 2011;200:2048–66.

[21] Givoli D. High-order local non-reflecting boundary conditions: A review. Wave Motion 2004;39:319–26.

[22] Lancioni G. Numerical comparison of high-order absorbing boundary conditions and perfectly matched layers for a dispersive one-dimensional medium. Comput Methods Appl Mech Engrg 2012;209-212:74–86.

[23] Basu U, Chopra AK. Perfectly matched layers for transient elastodynamics of unbounded domains. Internat J Numer Methods Engrg 2004;59:1039–74.

[24] Rabinovich D, Givoli D, Bécache E. Comparison of high-order absorbing boundary conditions and perfectly matched layers in the frequency domain. Int J Numer Methods Biomed Eng 2010;26:1351–69.

[25] Zerfa Z, Loret B. A viscous boundary for transient analyses of saturated porous media. Earthq Eng Struct Dyn 2004;33:89–110.

[26] Han B, Zdravkovic L, Kontoe S. Numerical and analytical investigation of compressional wave propagation in saturated soils. Comput Geotech 2016;75:93–102.

[27] Modaressi H, Benzenati I. Paraxial approximation for porelastic media. Soils Dyn Earthq Eng 1994;13:117–29.

[28] Degrande G, Roeck G. An absorbing boundary condition for wave propagation in saturated poroelastic media. Part I: Formulation and efficiency evaluation. Soils Dyn Earthq Eng 1993;12:411–21.

[29] Degrande G, Roeck G. An absorbing boundary condition for wave propagation in saturated poroelastic media. Part II: Finite element formulation. Soils Dyn Earthq Eng 1993;12:423–32.

[30] Akiyoshi T, Fuchida K, Fang HL. Paraxial approximation for porelastic media. Soils Dyn Earthq Eng 1994;13:387–97.

[31] Gajo A, Saetta A, Vitaliani R. Silent boundary conditions for wave propagation in saturated porous media. Int J Numer Anal Methods Geomech 1996;20:253–73.

[32] Fernandez Merodo JA, Mira P, Pastor M, Li T. GeHoMadrid user manual. Technical report- internal report, CEDEX (Madrid); 1999.

[33] Zienkiewicz OC, Chan AHC, Pastor M, Schrefler BA, Shiomi T. Computational geomechanics with special reference to earthquake engineering. Chichester: John Wiley & Sons; 1999.

[34] Zienkiewicz OC, Chang CT, Bettess P. Drained, undrained, consolidating and dynamic behaviour assumptions in soils. Geotechnique 1980;30(4):385–95.

[35] Zienkiewicz OC, Shiomi T. Dynamic behaviour of saturated porous media. The generalized Biot formulation and its numerical solution. Int J Numer Anal Methods Geomech 1984;8:71–965.

[36] Newmark NM. A method of computation for structural dynamics. J Eng Mech Div ASCE 1959;85:67–94.

[37] Arias-Trujillo J, Blazquez R, Lopez-Querol S. A methodology based on a transfer function criterion to evaluate time integration algorithms. Soils Dyn Earthq Eng 2012;37:1–23.

[38] Kouroussis G, Verlinden O, Conti C. Finite-dynamic model for infinite media: Corrected solution of viscous boundary efficiency. ASCE J Eng Mech 2011;137(7):509–11.

[39] Toshinawa T, Ohmachi T. Ground motion simulation by using simplified three-dimensional finite element method. In: Proceedings of the earthquake engineering, tenth world conference. Balkema, Rotterdam; 1992, p. 851–6.

[40] Verruijt A. Soil dynamics. Delft University of Technology; 2005.

[41] Kellezi L. Local transmitting boundaries for transient elastic analysis. Soil Dyn Earthq Eng 2000;19:533–47.

[42] Smith SW. The scientist and engineer's guide to digital signal processing. 502407 San Diego, CA, United States: California Technical Publishing; 1997.

[43] Bendat JS, Piersol AG. Random data: analysis and measurement procedures, Vol. 729. John Wiley & Sons; 2011.